

# Different Velocity Dependences of Physical Conditions of High- and Low-Ionization Lines in Broad-Line Regions

Stephanie A. Snedden

*Apache Point Observatory / New Mexico State University, 2001 Apache Point Rd.,  
Sunspot, NM 88349*

C. Martin Gaskell

*Dept. Physics and Astronomy, University of Nebraska, Lincoln, NE 68588*

## ABSTRACT

We present results from a study of high- and low-ionization emission line ratios as a function of projected velocity for a sample of eight active galactic nuclei (AGNs). Our results are based on analysis of high signal-to-noise optical and *Hubble Space Telescope (HST)* UV spectra. Comparing the emission line ratios to those predicted by photoionization models indicates that the physical conditions responsible for the high-ionization emission lines are consistent with a wind, whereas those of the low-ionization lines are consistent with a virialized disk.

## 1. Introduction

It is evident from reverberation mapping studies that high- and low-ionization emission lines in AGNs show different time-lag responses to continuum variability. Presumably, they are generated at different distances from the central engine (Korista et al; 1995, Santos-Lleó et al.; 1997, among others). However, it is still a matter of debate whether the kinematics of the high- and low-ionization regions are fundamentally different; e.g., is the high-ionization gas associated with a wind and the low-ionization gas with a disk? In this study we look for evidence of virialized motion from the emission lines of both high- and low-ionization gas of AGNs. We do this by looking at line ratios as a function of projected velocity across the emission line profiles.

## 2. Data and Analysis

For this study, we measured emission line ratios as a function of projected velocity for eight AGNs with high signal-to-noise optical and UV spectra. The sample is listed in Table

1. The optical spectra, provided by Giovanna Stirpe, include the H $\alpha$  and H $\beta$  lines. [S II]  $\lambda\lambda 6716, 6731$ , [N II]  $\lambda 6583$ , [O I]  $\lambda 6364$  + [Fe X]  $\lambda 6374$ , [O III]  $\lambda\lambda 4959, 5007$  were deblended from the Balmer lines, the narrow-line components were removed, and a power law continuum was subtracted, all as described in Stirpe, 1991. The *HST FOS* UV spectra were deblended of N V  $\lambda 1240$ , Al III]  $\lambda 1857$ , Si III]  $\lambda 1892$ , and a local power law continuum was subtracted from the Ly $\alpha$  to C III] region. Next, we integrated all emission line fluxes over a high-velocity component centered at  $\pm 4000 \text{ km} \cdot \text{s}^{-1}$ , an intermediate-velocity component centered at  $\pm 2000 \text{ km} \cdot \text{s}^{-1}$  and a low-velocity component centered at  $0 \text{ km} \cdot \text{s}^{-1}$ . The ratios Ly $\alpha$ /H $\alpha$ , H $\beta$ /H $\alpha$ , Ly $\alpha$ /C IV and C III]/C IV for each velocity component were then calculated. We used *CLOUDY* v90.04 (Ferland et al.; 1998) to generate grids of emission line ratios as a function of hydrogen density,  $n_H$ , and surface photon flux capable of ionizing hydrogen,  $\Phi_H$ . The measured emission line ratios were compared to the predicted values to determine  $n_H$  and  $\Phi_H$  as a function of velocity for the objects in our sample.

Figures 1 and 2 show  $n_H$  and  $\Phi_H$  averaged over the objects in our sample, normalized to the value for the low velocity gas. Figure 1 shows the predicted physical conditions as a function of velocity for the low-ionization gas, as deduced from the hydrogen lines. Note that the normalized surface photon flux is plotted to the one-fourth power. If the photon flux ratio is linear with respect to the absolute value of the velocity in this plot, it implies the line-emitting gas obeys the inverse-square law. Figure 2 shows the same for the high-ionization gas, as deduced from the carbon lines and Ly $\alpha$ . However, for this case, the normalized surface photon flux is *not* raised to the one-fourth power, since  $\Phi_H$  is constant with respect to velocity for the high-ionization gas. In all figures the errorbars show cumulative errors, including scatter in the average ratios across the sample as well as uncertainty in the physical conditions as deduced by matching observed line ratios to the photoionization models. The latter error results from uncertainties in deblending and continuum subtraction.

### 3. Discussion

A comparison of Figures 1 and 2 shows a fundamental difference in the photoionization model predictions of physical conditions of the low- and high-ionization gas. The low-ionization Balmer-line-emitting gas (Figure 1), shows a clear change in both  $n_H$  and  $\Phi_H$  as a function of velocity. The higher velocity gas is denser than low velocity gas. There is also a trend toward higher  $\Phi_H$  as projected velocity increases, and the trend fits the inverse-square law within the errors. The high-ionization gas, however, shows no such trend (Figure 2). Both  $n_H$  and  $\Phi_H$  are constant as a function of projected velocity.

| Object       |
|--------------|
| B2 2201+31A  |
| Fairall 9    |
| NGC 3783     |
| NGC 5548     |
| PG 1116+215  |
| PG 1211+143  |
| PG 1351+640  |
| Pks 2251+113 |

Table 1: The sample.

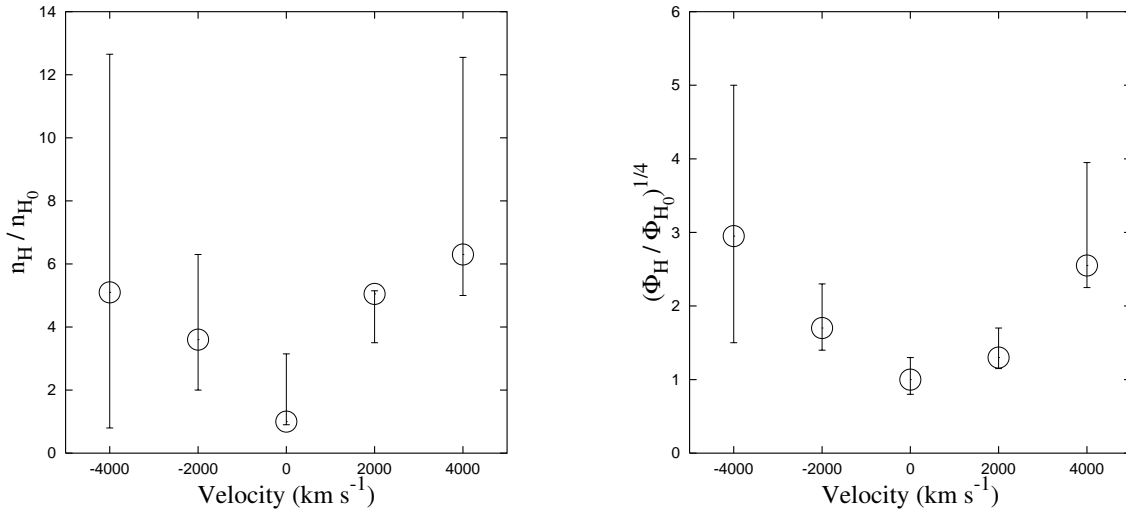


Fig. 1.— *a*) Average density,  $n_H$ , for the entire sample, deduced from hydrogen lines and normalized to the low velocity value,  $n_{H_0}$ , as a function of velocity. *b*) Average surface photon flux,  $\Phi_H$ , for the entire sample, deduced from hydrogen lines and normalized to the low velocity value,  $\Phi_0$ , as a function of velocity. We plot this ratio to the one-fourth power.

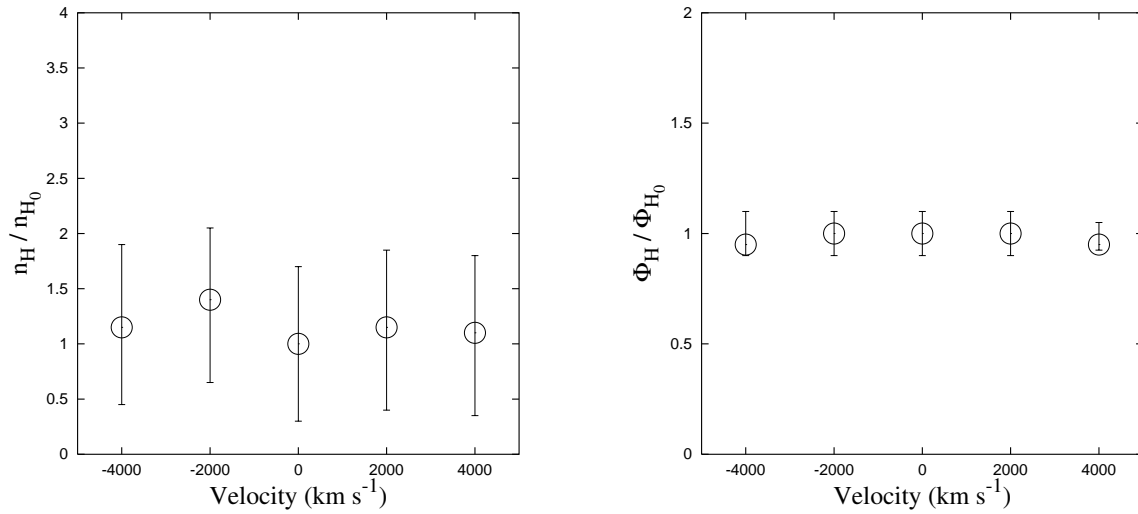


Fig. 2.— *a*) Average density,  $n_H$ , for the entire sample, deduced from high-ionization lines and normalized to the low velocity value,  $n_{H_0}$ , as a function of velocity. *b*) Average surface photon flux,  $\Phi_H$ , for the entire sample, deduced from high-ionization lines and normalized to the low velocity value,  $\Phi_0$ , as a function of velocity.

#### 4. Conclusions

The results shown in Figure 1 are consistent with the Balmer line emitting gas being virialized. The lower velocity low-ionization gas sees a smaller  $\Phi_H$  in accord with the inverse-square law. Figure 2, however, is evidence of fundamentally different kinematics for the high-ionization gas that produces C IV. In this case, the independence of physical conditions with respect to projected velocity, averaged over the sample, is consistent with gas motion that is not virialized.

These results are consistent with the high-ionization lines arising in a wind and the low-ionization lines arising in a disk.

#### REFERENCES

- Ferland, G. J. et al. 1998, PASP , 110, 761  
Korista, K.T. et al. 1995, ApJS , 97, 285  
Santos-Lleó, M. et al. 1997, ApJS ,112, 271  
Stirpe, G. M. 1991 A&A , 247, 3S